Applied Physics Letters

RESEARCH ARTICLE | AUGUST 08 2024

Velocity of subsonic and hypersonic surface acoustic waves on silicon with native oxide layer

Fehima Ugarak ; Alexis Mosset ; Vincent Laude

Appl. Phys. Lett. 125, 062201 (2024)
https://doi.org/10.1063/5.0210667

Applied Physics Letters ARTICLE pubs.aip.org/aip/apl

Velocity of subsonic and hypersonic surface acoustic waves on silicon with native oxide layer

Cite as: Appl. Phys. Lett. **125**, 062201 (2024); doi: 10.1063/5.0210667
Submitted: 26 March 2024 · Accepted: 29 July 2024 ·
Published Online: 8 August 2024

View Online Export Citation CrossMark

Fehima Ugarak, Alexis Mosset, and Vincent Laude[a)]

AFFILIATIONS

Université de Franche-Comté, CNRS, Institut FEMTO-ST; 15B avenue des Montboucons, 25030 Besançon, France

[a)]Author to whom correspondence should be addressed: vincent.laude@femto-st.fr

ABSTRACT

The anisotropic dependence of the velocity of surface acoustic waves (SAW) on silicon is explored using surface Brillouin light scattering. Measurements of the SAW velocity are compared to a numerical model that takes into account the native thin amorphous oxide layer formed at the top surface of the silicon wafer. The model accounts for material loss and provides a relative estimate for the backscattered intensity resulting from the ripple effect. For the (100) sample considered, a thickness of 4 nm fits well with experimental data, considering material constants of amorphous silica for the oxide. A global phase velocity decrease of −11 m/s per nanometer of silica thickness is predicted for surface phonons at frequencies around 16 GHz.

Surface acoustic waves (SAW) are collective excitations propagating along the surface of a solid material. They enter physical phenomena, such as thermal transport,[1] are useful in materials science,[2] and are technologically important for applications in information communication technology.[3] In this work, we specifically consider silicon as the propagation substrate, but methods and results could be extended to other opaque crystalline solids. SAW propagation velocity on bare silicon is anisotropic but non-dispersive. The velocity curve as a function of the angle ψ of propagation in the plane of the surface combines two branches, with velocities of the order of 5000 m/s, as shown in Fig. 1. The branch labeled A is the slowest; it supports a subsonic[4] SAW. The branch labeled B supports a leaky surface acoustic wave (leaky-SAW) with some radiation loss that depends on the propagation angle ψ. A quasi-shear bulk acoustic wave (QS-BAW) coexists with the surface waves and leads to the formation of the anti-crossing between branches A and B.

The velocity of SAW on silicon has been determined experimentally by different techniques operating in different frequency ranges. Ultrasonic measurements were reported by Tarasenko *et al.*[5] for frequencies of the order of 200 MHz. The measurement technique they used is the laser acoustic method (LAM), whereby the SAW phase velocity on bare silicon was determined at low frequencies. The resulting experimental data for phase velocity, shown with star markers in Fig. 1(b), fit well with theory, and both branches of the velocity curve can be identified. The surface Brillouin light scattering (SBLS) measurements reported by Sandercock[6] and then Stoddart *et al.*[7] suggested slightly lower SAW velocities. The SBLS technique detects thermal, spontaneous surface phonons in the hypersonic frequency range ($\approx$ 16 GHz in our own experiment). The experimental velocities reported by Stoddart *et al.*,[7] shown with square markers in Fig. 1(b), are apparently slower by about 1% compared to theory. Our surface BLS measurements, shown with filled square markers in Fig. 1(b), are similar to Stoddart's and confirm them. The discrepancy may seem small but is actually larger than the standard deviation of the fit to the measurements, which we estimate to be around 0.2%.

Sandercock suggested that there are potential differences in elastic constants near the surface compared to those in the bulk material.[6] Stoddart *et al.*[8] explored numerically this effect by considering the native oxide layer, as well as various other corrections to the experimentally determined SBLS frequencies, but could not fully explain the discrepancies. In particular, the anti-crossing as a function of the in-plane angle was not reproduced. In the following, we indeed explain the apparent slowing down of high-frequency SAW on silicon by the presence of a thin layer of silica, resulting from the native oxidation of silicon at room temperature. A numerical model of the dispersion relation for surface phonons that considers an arbitrary variation of material constants with depth is proposed, based on recent developments around the quasinormal mode description of elastic waves or acoustic phonons.[9] Given the high phonon frequencies involved, around 16 GHz, the phonon wavelength λ is of the order of 300 nm. The apparent slowing-down observed in SBLS measurements is found to be compatible with a silica thickness of about 4 nm, or $\lambda/75$.

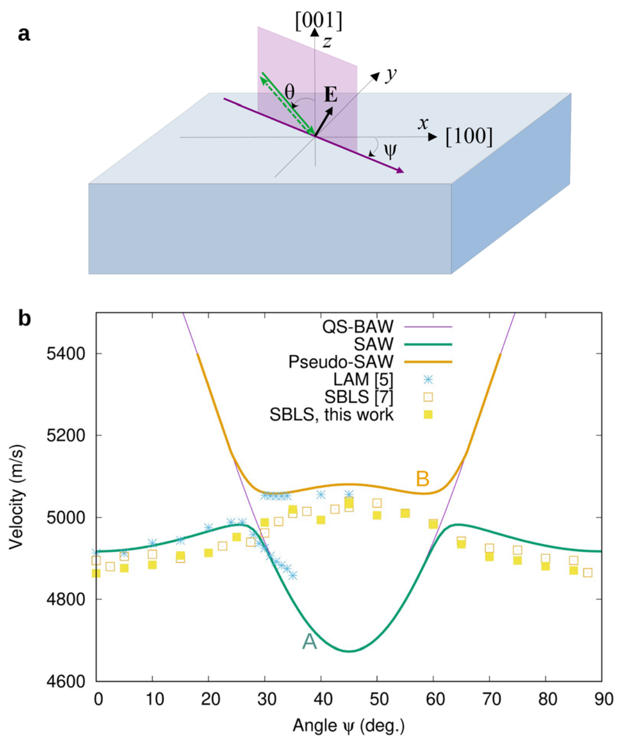

FIG. 1. Velocity curves for elastic waves on bare Si(001). (a) The configuration considered is sketched, with incident light figured by the green solid arrow and backscattered light with the green dotted arrow. The electric field vector **E** is in the plane of incidence. θ is the angle of incidence. Elastic waves propagate with an angle ψ along the (001) surface. (b) Phase velocity is shown vs angle ψ. The dispersion relation involves a quasi-shear bulk acoustic wave (QS-BAW), a subsonic SAW, and a leaky-SAW. Experimental data by Tarasenko *et al.* (LAM),[5] Stoddart *et al.* (SBLS),[7] and ourselves (SBLS) are added with markers.

SBLS was used to measure the SAW velocity on a n-doped silicon substrate. SBLS plays a crucial role in the determination of the elastic properties of materials that are either opaque or nearly opaque. In this case, indeed, the substantial optical absorption limits the penetration depth of the laser, confining it to a small volume near the surface. As a result, SBLS is widely used to study the physical properties of thin films,[10,11] interfaces,[12] and layered materials.[10,13,14]

In the backscattering configuration depicted in Fig. 1(a), the incidence angle is θ and the optical wavenumber is $k = 2\pi/\lambda_0$ with $\lambda_0 = 532$ nm. Only surface phonons with in-plane wavenumber $q = 2k \sin\theta$ contribute to light scattering. The shape of the Brillouin peak is a Lorentzian function, centered on a frequency f_B, whose width depends on the phonon lifetime. The phase velocity v of surface phonons is related to the frequency shift by $v = \lambda_0 f_B/(2\sin\theta)$. Surface phonons modulate the height of the free surface, causing it to deviate from a perfectly flat plane. This dynamical corrugation of the surface, or ripple effect,[15] results in the inelastic scattering of incident light. The intensity of the scattering process depends on the reflectivity of the surface and is only effective for the normal component u_z of the phonon displacement field. Laser light is polarized in the incidence plane (p-pol), since for sagittally polarized SAW, this choice maximizes the ripple effect.[16] The measurements reported here are made at a power of around 160 mW. For sending and collecting backscattered light from the sample, a lens with a numerical aperture ≈ 0.1 was used. It has been shown[6,16] that the precision of determining the SAW velocity and attenuation through SBLS is affected by the limited aperture of the collection lens. Due to the low signal intensity, employing a collection lens with a substantial aperture is necessary to perform the analysis of a sufficient amount of scattered light. According to Elmiger *et al.*,[17] the backscattered intensity for silicon displays a maximum value for angle of incidence $\theta \approx 60°$. Since measured phase velocities are very sensitive to the value of angle of incidence, its value must be precisely estimated. The angle of incidence was set to $\theta = 59.5°$, while the sample was rotated around the normal to the surface to change the angle ψ from 0° to 90° with a step of 5°. The spectrum of the scattered light was analyzed using a six-pass Tandem Fabry–Pérot interferometer (Table Stable LTD., model TFP-2 HC) with mirror spacing set to 6 mm and scanning amplitude to 450 nm. The number of cycles for each measured point was 10 000, about 2 h of acquisition time. Some examples of experimental Brillouin peaks and a fit example are reported in Fig. 2.

The traditional method to obtain the dispersion relation of surface waves on solids is to represent the wave as a linear superposition of three partial waves and to look for the zero or the minimum of the boundary condition determinant expressing that the surface traction vanishes. This method was used to obtain the dispersion relation of Fig. 1(b) and can be extended to layered substrates, whereby propagation becomes dispersive in addition to anisotropic.[8]

As an alternative, we compute the resolvent map of the dispersion relation.[18] The principle is to prepare a one-dimensional mesh of the layered substrate, with material constants varying along the z-axis, to apply a spatially random excitation to the top layer and to solve the elastodynamic equation for all wavenumber-frequency pairs (q, f) using the finite element method.[19] The resolvent map is formed by plotting the total energy of the solution, or its log-derivative with

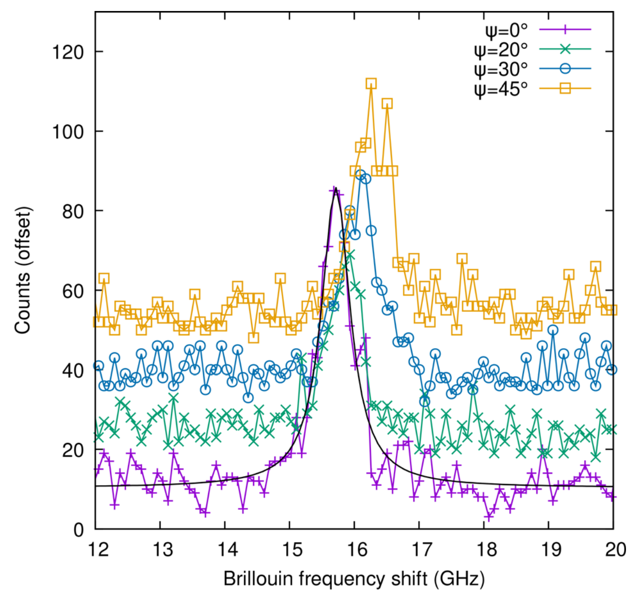

FIG. 2. Brillouin peaks measured for incidence angle $\theta = 59.5°$, for some values of the azimuthal angle ψ. Spectra are vertically offset to ease reading. A Lorentzian fit example is shown with the solid line for azimuthal angle $\psi = 0°$.

respect to frequency, in order to reveal all resonances (poles and damped poles).[18] With this approach, both SAW and leaky-SAW are reinterpreted as quasinormal guided waves:[9] if desired, their complex frequency can be obtained as a function of the wavenumber, with the imaginary part accounting for propagation damping. There is no need to assume *a priori* the existence of modes of propagation or to solve an eigenvalue problem, however, since all surface excitations will be present in the response to the surface excitation.

Figure 3(a) presents the dispersion relation for surface phonons in the case of a thin layer of silica (thickness $h = 4$ nm) above the silicon substrate, obtained with the technique just described.[20] There are mainly two dispersion branches, labeled A and B, respectively. Compared to Fig. 1, they are both shifted to lower velocities by approximately −45 m/s. The agreement of numerical dispersion with the SBLS experimental points is rather good. Examples of the distribution of displacements with depth are shown in Fig. 3(b) for a few propagation angles.

The lower branch A is again subsonic and supports generalized Rayleigh waves. Those are elliptically polarized in the sagittal plane defined by the propagation vector **q** and the normal to the surface. The velocity first increases with angle ψ until it interacts with the QS-BAW, with which it forms an anti-crossing somewhere between waves A2 and A3. The variations of displacements with depth for wave A3, in particular, show that the surface wave extends significantly inside the substrate, i.e., that it delocalizes. The displacements amplitudes decay exponentially in the direction perpendicular to the surface for all angles, except for $\psi = 45°$ (wave A4) at which point the solution is completely delocalized and becomes a surface skimming bulk wave (SSBW).

The upper branch B is supersonic and hence expected to support leaky surface waves. The displacements for wave B2 are clearly dominated by the QS-BAW. Starting from the anti-crossing, the displacements distribution transforms more and more into that of a Rayleigh SAW. For $\psi = 45°$ (wave B4), the conversion is complete and the solution is a bound state in the continuum (BIC),[21] completely uncoupled from the QS-BAW.

The experimental phase velocities closely follow the Rayleigh wave branch A up to an azimuthal angle ψ of about 25° but subsequently follow the leaky SAW branch B. In order to explain this fact, we observe that the ripple effect involves only the normal displacement amplitude u_z near the surface.[15] Since the observed surface phonons are of thermal origin, their total energy is proportional to $k_B T$ and distributes in the depth. Hence, we expect to detect preferably those phonons that are confined at the surface, whose polarization is dominated by the surface value of $|u_z|$. We evaluated numerically the surface displacement power spectrum,[15] as reported in Fig. 4, by computing the quantity $I = \langle |u_z|^2 \rangle$, i.e., the integrated squared vertical displacement in the oxide layer. Material loss inside silicon is now included by the consideration of the phonon viscosity tensor for silicon, turning the elastic tensor into a frequency-dependent complex tensor.[9] As a note, without material loss, the resonance would diverge at the Brillouin frequency and the characteristic damped Lorentzian response function would not be observed; Loudon's original Green's function formulation of the ripple effect[15] did not include this correction. In practice, the phonon viscosity tensor for silicon[22] was multiplied by a factor 10 since otherwise the Lorentzian peak width was underestimated compared to the experiment. Hence, there are other factors leading to peak broadening in addition to material loss. Figure 4 illustrates how the SBLS response jumps from the lowest branch A to the upper branch B across the anti-crossing. The numerical result is overall consistent with the experimental observations in Fig. 2, though we did not attempt to integrate over the finite range of phonon wavenumbers that is spanned in the experiment.

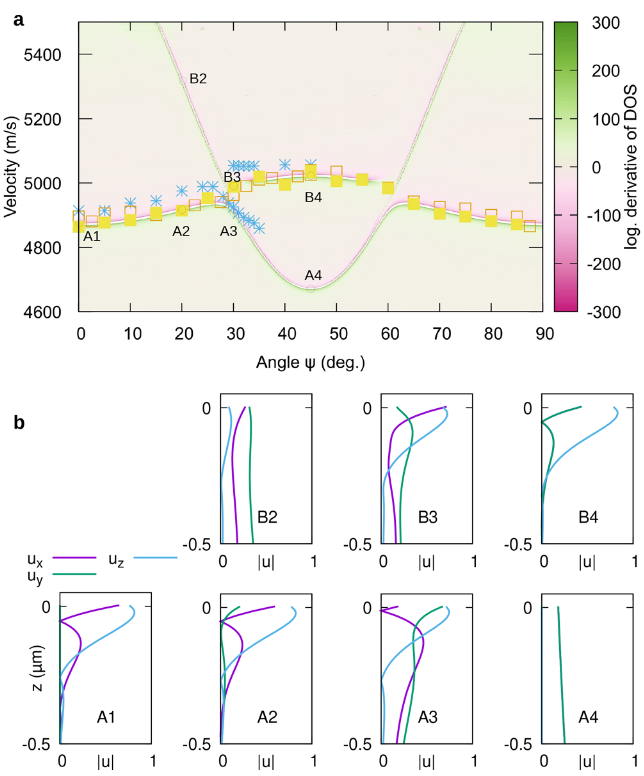

FIG. 3. Numerical analysis by the resolvent map. (a) Velocity is shown vs in-plane angle ψ, for a layer of silica with thickness $h = 4$ nm on top of Si(001). The surface phonon wavenumber $q = 4\pi \sin(\theta)/\lambda_0$ is imposed by the backscattering configuration. The logarithmic derivative of the density of states (DOS) is displayed on the color scale. Markers are for experimental data by Tarasenko *et al.*[5] (blue stars), Stoddart *et al.*[7] (empty orange squares), and ourselves (filled yellow squares). (b) Variation of displacements is shown vs depth, for selected waves.

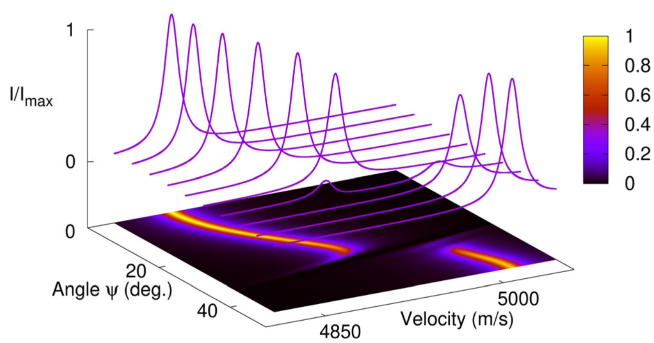

FIG. 4. Surface displacement power spectrum of a Si(001) substrate with 4 nm of native oxide, computed as the squared vertical displacement of the response to a random excitation body force within the oxide layer. Frequency cross sections are shown as a function of in-plane angle ψ every 5°.

As a note, why the ultrasonic measurements reported by Tarasenko *et al.*[5] agree with the computations for a bare silicon wafer can be understood by evaluating the phonon wavelength. Given that in the ultrasonic case $\lambda = v/f$ with a frequency of $f \ll 200$ MHz, the phonon wavelength is $\lambda \gg 25$ μm. In this case, the ratio h/λ is very small and the presence of the oxide layer can be neglected. In their experiments, indeed, Tarasenko *et al.*[5] mentioned that the dispersion curves have a very small tilt, indicating the presence of a thin native oxide layer, whose thickness they estimate to be about 2–5 nm. Conversely, in the SBS case, $\lambda = \lambda_0/(2\sin\theta) \approx 300$ nm and $h \approx \lambda/75$. Our numerical results indicate a decrease of −11 m/s per nanometer of amorphous silica, rendering the slowing down of surface phonons noticeable even for a very thin layer of native oxide.

High-resolution transmission electron microscopy (HRTEM; Thermo Fisher Talos F200X) was used independently to estimate the thickness of the oxide layer.[23] For this purpose, the sample was first covered with a protective layer of Pt before being cut with a focused ion beam (FIB; Thermo Fisher Scios2). Using the Velox software, the average SiOx layer thickness was estimated from ten different micrographs to be 3.54 ± 0.32 nm. This result agrees fairly well with our estimated 4 nm thickness for an equivalent layer of silica. We finally observe that our results are also consistent with the value $h = 4.23 \pm 0.13$ nm that was reported for the oxide layer forming on the surface of a silicon sphere.[24]

The authors acknowledge fruitful discussions with Nicolas Martin. They are indebted to Antonio J. Santos Izquierdo-Bueno, Juan J. Jimenez Rios, and Francisco M. Morales Sanchez for HRTEM measurements at the University of Cadiz, Spain. This work has been supported by the EIPHI Graduate School (Contract No. ANR-17-EURE-0002) and by the Bourgogne-Franche-Comté Region. Support from the French Renatech network and its FEMTO-ST technological facility is also gratefully acknowledged.

AUTHOR DECLARATIONS

Conflict of Interest

The authors have no conflicts to disclose.

Author Contributions

Fehima Ugarak: Conceptualization (equal); Data curation (lead); Investigation (lead); Methodology (equal); Resources (equal); Validation (equal); Visualization (supporting); Writing – original draft (equal); Writing – review & editing (supporting). **Alexis Mosset:** Data curation (supporting); Funding acquisition (supporting); Methodology (equal); Resources (equal); Supervision (equal); Validation (equal); Writing – review & editing (supporting). **Vincent Laude:** Conceptualization (equal); Funding acquisition (lead); Methodology (equal); Project administration (lead); Software (lead); Supervision (equal); Validation (equal); Visualization (equal); Writing – original draft (equal); Writing – review & editing (lead).

DATA AVAILABILITY

The data that support the findings of this study are available from the corresponding author upon reasonable request.

REFERENCES

1. M. Nomura, R. Anufriev, Z. Zhang, J. Maire, Y. Guo, R. Yanagisawa, and S. Volz, "Review of thermal transport in phononic crystals," Mater. Today Phys. **22**, 100613 (2022).
2. P. Hess, "Surface acoustic waves in materials science," Phys. Today **55**(3), 42–47 (2002).
3. K.-Y. Hashimoto, *Surface Acoustic Wave Devices in Telecommunications* (Springer, 2000), Vol. 116.
4. Subsonic surface waves are slower than any bulk acoustic wave in the material. They are hence truly guided at the surface.
5. A. Tarasenko, R. Čtvrtlík, and R. Kudělka, "Theoretical and experimental revision of surface acoustic waves on the (100) plane of silicon," Sci. Rep. **11**, 2845 (2021).
6. J. R. Sandercock, "Light scattering from surface acoustic phonons in metals and semiconductors," Solid State Commun. **26**, 547–551 (1978).
7. P. R. Stoddart, J. D. Comins, and A. G. Every, "Brillouin-scattering measurements of surface-acoustic-wave velocities in silicon at high temperatures," Phys. Rev. B **51**, 17574 (1995).
8. P. R. Stoddart, J. C. Crowhurst, A. G. Every, and J. D. Comins, "Measurement precision in surface Brillouin scattering," J. Opt. Soc. Am. B **15**, 2481–2489 (1998).
9. V. Laude and Y.-F. Wang, "Quasinormal mode representation of radiating resonators in open phononic systems," Phys. Rev. B **107**, 144301 (2023).
10. G. Carlotti, "Elastic characterization of transparent and opaque films, multilayers and acoustic resonators by surface Brillouin scattering: A review," Appl. Sci. **8**, 124 (2018).
11. L. Bassoli, F. Nizzoli, and J. R. Sandercock, "Surface Brillouin scattering in polycrystalline gold," Phys. Rev. B **34**, 1296 (1986).
12. R. Jorna, D. Visser, V. Bortolani, and F. Nizzoli, "Elastic and vibrational properties of nickel films measured by surface Brillouin scattering," J. Appl. Phys. **65**, 718–725 (1989).
13. H. Xia, X. K. Zhang, K. J. Chen, G. X. Cheng, D. Feng, G. Socino, L. Palmieri, G. Carlotti, D. Fioretto, and F. Nizzoli, "Surface Brillouin scattering in semiconductor Fibonacci multilayers," Phys. Rev. B **42**, 11288 (1990).
14. R. Zanoni, J. A. Bell, G. I. Stegeman, and C. T. Seaton, "Brillouin spectroscopy of multilayer films," Thin Solid Films **154**, 225–237 (1987).
15. R. Loudon, "Theory of surface-ripple Brillouin scattering by solids," Phys. Rev. Lett. **40**, 581 (1978).
16. P. Mutti, C. E. Bottani, G. Ghislotti, M. Beghi, G. A. D. Briggs, and J. R. Sandercock, "Surface Brillouin scattering—Extending surface wave measurements to 20 GHz," in *Advances in Acoustic Microscopy* (Springer, 1995), Vol. 1, pp. 249–300.
17. M. W. Elmiger, "Raman scattering under high pressure in samariumselenide and Brillouin spectroscopy from surface acoustic waves," Ph.D. thesis (ETH Zurich, 1988).
18. V. Laude and M. E. Korotyaeva, "Stochastic excitation method for calculating the resolvent band structure of periodic media and waveguides," Phys. Rev. B **97**, 224110 (2018).
19. L. L. Spina, Q. Micard, A. Mosset, S. Margueron, A. Bartasyte, and V. Laude, "Dispersion of surface elastic waves on Z-$LiNbO_3$ films on Z-sapphire," Appl. Phys. Lett. **122**, 172202 (2023).
20. Independent elastic constants for silicon are $c_{11} = 165.7$ GPa, $c_{12} = 63.9$ GPa, and $c_{44} = 79.62$ GPa; mass density is $\rho = 2331$ kg/m^3. Independent elastic constants for silica are $c_{11} = 78.5$ GPa and $c_{44} = 31.2$ GPa; mass density is $\rho = 2203$ kg/m^3.
21. C. W. Hsu, B. Zhen, A. D. Stone, J. D. Joannopoulos, and M. Soljačić, "Bound states in the continuum," Nat. Rev. Mater. **1**, 16048 (2016).
22. Independent components of the viscosity tensor for silicon are taken as $\eta_{11} = 0.53$ mPa s, $\eta_{12} = 0.2$ mPa s, and $\eta_{44} = 0.25$ mPa s.
23. A. J. Santos Izquierdo-Bueno, J. J. Jimenez Rios, and F. M. Morales Sanchez, private communication (2024).
24. J. Zhang, Y. Li, X. Wu, Z. Luo, and H. Wei, "Determining mean thickness of the oxide layer by mapping the surface of a silicon sphere," Opt. Express **18**, 7331–7339 (2010).